JOURNAL OF SPACECRAFT AND ROCKETS
Vol. 44, No. 1, January–February 2007

High-Fidelity Gravity Offloading System for Free–Free Vibration Testing

Gyula Greschik*
University of Colorado, Boulder, Colorado 80309
and
W. Keith Belvin†
NASA Langley Research Center, Hampton, Virginia 23681

DOI: 10.2514/1.21454

Proposed for the high performance vibration testing of free-flying systems is the Marionette paradigm, a mechanically simple passive gravity compensation scheme characterized by low mass, little interference with specimen response, high imperfection tolerance, and compatibility with up to medium scale specimen kinematics. An introduction to this concept, theory, features, and some practicalities, is offered. The need for and the potential of system optimization are discussed and illustrated. Possible means to generalize the basic concept to adaptive specimen geometries or to the simulation of nonuniform inertial conditions are also discussed. Hardware and numerical illustrations are presented.

Nomenclature

d	=	diameter
dz	=	vertical displacement
E, ν	=	Young's modulus and Poisson's ratio
e	=	fulcrum offset
e_x, e_z	=	fulcrum offset components in directions x, z
h	=	fly beam arm tip vertical displacement
K_α	=	geometric nonlinear stiffness against beam tilt
L	=	fly beam span: the distance between arm endpoints
M	=	moment
m	=	mass
m_+	=	direct mass overhead = support structure mass/mass supported
r	=	fly beam arm length
S, S_i	=	load tree top and anchor point forces
W, w	=	weight
λ	=	fly beam arm ratio $=r_1/r_2$
ρ	=	density (specific mass)
ϕ	=	Force ratio: ratio of fly beam arm loads $=S_1/S_2$

Subscripts

1, 2	=	association with one or the other fly beam arm

I. Introduction

FOR the cost effective hardware verification of ever larger, lighter, and more compliant space structures (antennas, booms, sunshades, solar sails, etc.), increasingly high fidelity and sensitivity is required of the laboratory simulation of weightlessness. High fidelity and sensitivity, however, also imply vulnerability to gravity effects and to the imperfections of both specimen and testing apparatus.

To effectively balance fidelity against vulnerability to imperfections in the context of current engineering practice (in which numerical simulation and testing are complementary), a test setup must strictly limit nondeterministic effects (random slip, friction, damping). The alleviation of deterministic effects which can be precisely quantified (such as added inertia) is often a secondary goal, as these can be properly modeled numerically. Robustness against imperfections must also be provided.

An effort to seek alternatives to existing technology led to the development of the herein proposed Marionette paradigm wherein the weight of each part of the specimen is balanced by the other parts. Mass overhead, contributed to by light fly beams and suspension cords only, is low, often negligible, and is precisely known. Damping, friction, and slip are eliminated, and specimen response is not affected by deleterious material stiffness. Deleterious second order (geometric) stiffness effects can be eliminated with a precision limited only by the accuracy of geometric measurement. The architecture to achieve these qualities is simple, with few limitations on its overall design and with high tolerance against both specimen and support system imperfections. Kinematics can naturally involve up to moderate specimen displacements and deformations in both the vertical and horizontal directions. The concept can also be generalized to accommodate some adaptive model geometries, and the simulation of inertial loading conditions in weightlessness, for example, steady state acceleration, is also possible. This unique combination of high performance, fault tolerance, mechanical simplicity, and design flexibility are an attractive alternative to "classic" gravity compensation schemes.

A. Gravity Compensation

Gravity is ubiquitous in everyday life on the global mechanical scale, rendering the human experience of weightlessness and the direct study of this condition impossible on Earth. Accordingly, ground tests to explore the *zero-g* performance of mechanical systems inevitably employ various compromise solutions. In fact, the set of means to negotiate such compromises is rich; it can be discussed from several different perspectives.

One way to classify schemes to eliminate gravity effects is in terms of the means employed. For example, one can distinguish [1,2] physical, buoyancy, pneumatic (air cushion and bearing), and mechanical methods. (The first category, "physical approach," includes parabolic flight and drop tests, not really gravity compensation but, in fact, orbital tests with Earth-colliding orbits.)

A broader categorization can be based on the dimensionality of the specimen motion accommodated [3]. Accordingly, one can

Presented as Paper 1839 at the 46th Structures, Structural Dynamics, and Materials Conference, Austin, TX, 18–21 April 2005; received 29 November 2005; revision received 18 May 2006; accepted for publication 31 May 2006.

*Research Associate, Center for Aerospace Structures, Department of Aerospace Engineering Sciences, USB 429, Member AIAA.

†Chief Engineer for Space, Structures and Materials Competency, 4 West Taylor Street/MS 230, Associate Fellow AIAA.

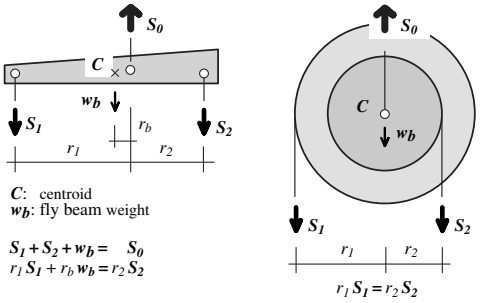

Fig. 1 Fly beam; wheel and axle.

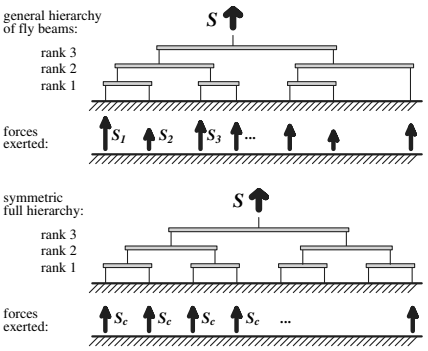

Fig. 2 Load tree; whiffle tree.

distinguish support systems to permit linear, planar, or spatial kinematics.

One can also rank gravity offloading options based on apparatus complexity. The simplest route is to avoid offloading altogether and downscale [4] until, according to constant thickness [5] or classic proportional [6] scaling principles, gravity effects reduce to tolerable levels. This approach is practical if sensitivity and quantitative fidelity are not critical. The next level of complexity, applicable to sufficiently stiff systems, is specimen alignment with the gravity field to eliminate direct gravitational bending. Further raising complexity, a horizontal specimen orientation free from nonlinear effects may be used with simply distributed lateral support, realized with cord-and-pulley mechanisms, counterweights, soft (so-called constant force) springs or "bungee" cords, pneumatic or buoyant bearing, etc. Such simple support generally affects and sometimes severely restricts specimen response. Finally, autonomous force control can be employed at each supported location. Depending on sensitivity and kinematic scope, the simulation of weightlessness can asymptotically approach perfection and/or can permit large kinematics. Hybrid active–passive control systems that combine robustness with high fidelity may offer the best performance [7,8].

One may observe that the cost of quality is the sophistication of support. It turns out, however, that high performance can also be achieved for many vibration problems with the simple scheme herein proposed: a single fly beam hierarchy.

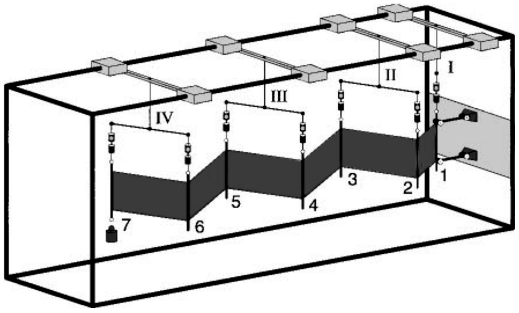

Fig. 3 Solar array deployment test setup, [1].

B. Fly Beams in Hardware Testing

Static determinacy and simplicity make the fly beam a convenient component in support and loading apparatus, more so than the wheel and axle, a mechanically equivalent but heavier alternative that accommodates large motion, Fig. 1. The repetitive hierarchical application of this element produces a load or a whiffle tree, the latter the special case with full symmetry and uniform geometry, Fig. 2, Load trees are typically used to mechanically control the application to a specimen of a desired force set; if weight effects are minor, then tree geometry defines force distribution which is scaled by the force **S** at the top of the hierarchy. Loads are exerted with such load trees, for example, in aircraft testing. An example for whiffle tree application is the rigorously uniform tensioning of film sheets [9].

Fly beams are typically used in specimen support (rather than loading) to simplify the apparatus by reducing the number of external support locations, as in the case of the solar panel deployment test by Fischer [1], Fig. 3. An example with multiple fly beam hierarchies is the PowerSail deployment experiment [10], Figs. 4a and 4b.

Fly beams are also used to directly aid gravity balancing with extra weights, as for the recent testing at NASA Langley Research Center of the L'Garde Encounter/ISP solar sail boom [11], Fig. 5. In this role, the beams serve as "frictionless pulleys" to reduce nondeterministic effects.

C. Single Point Suspension

As illustrated above, fly beams and load trees in testing are traditionally applied to *parts* of the structure and merely to simplify apparatus or procedure. The Marionette concept is a paradigmatic shift from this approach: it entrusts the support of the *entire* specimen to *one single* fly beam hierarchy and it consequently exploits the unique mechanical and kinematic features of this structure, described later.

The recognition and exploitation of these unique characteristics (which disappear if multiple external support locations are used) are critical to the new paradigm. Indeed, singular suspension hierarchies have been used before without recognizing and exploiting their kinematic uniqueness: large objects are occasionally gripped by construction or other cranes via multiple fly beams to guarantee a safe load distribution. A special example is the hoisting device with triangular load distribution elements, three dimensional versions of

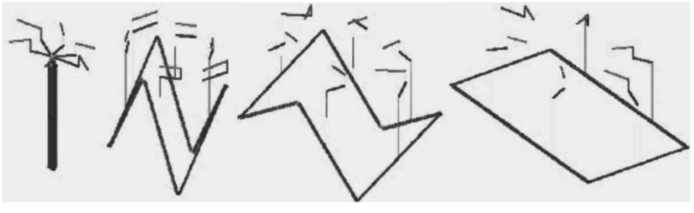

a) Deployment and support scheme

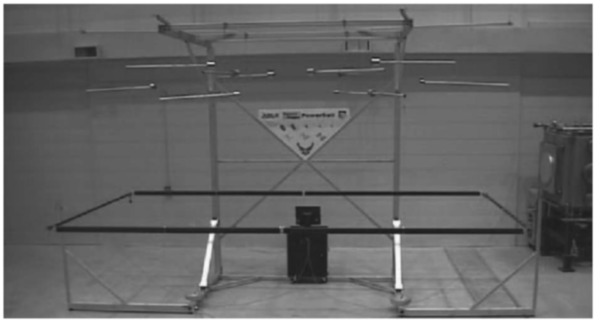

b) Deployed hardware

Fig. 4 Deployment test for PowerSail unit; figures taken from [10].

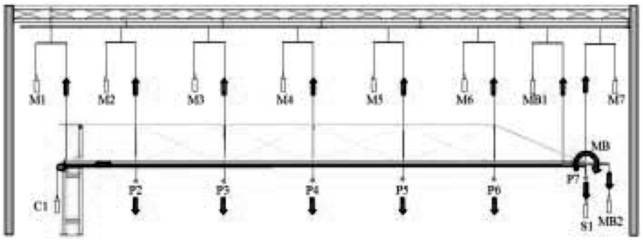

Fig. 5 Solar sail boom suspension, from [11].

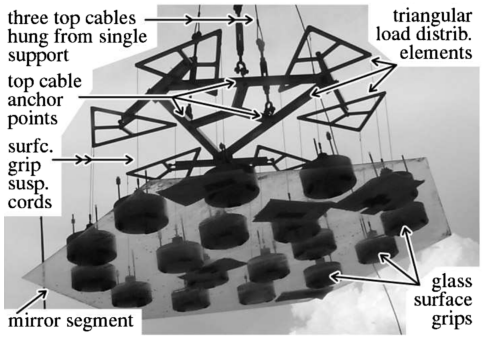

Fig. 6 Device to lift mirror shell (University of Arizona Mirror Laboratory, courtesy of J. Burge and B. Cuerden).

the fly beam, in Fig. 6 to handle a precision curved glass shell at the University of Arizona.

II. Marionette Paradigm

According to the Marionette paradigm, a specimen is suspended by a set of fly beams integrated into a single hierarchy, suspended from one external location. By virtue of the single external support, the specimen is subjected to only one constraint: its center of gravity (c.g.) is maintained stationary in space. This condition is equivalent to weightlessness with a fidelity defined by the geometry of support hierarchy. No additional constraints are imposed on the specimen within the limits of small to moderate kinematics. Further, the fly beam system has no frictional components or elastically adaptive parts, leaving no room for damping and material stiffness effects to occur. Fly beam and cord mass inertias are negligible in many cases and can be efficiently minimized in others.

A. Suspension with a Fly Beam Hierarchy

A load tree can exert any force set $\mathbf{S}_i$ with a nonzero resultant $\mathbf{S}$, Fig. 2, if its geometry and the force at its top are appropriately defined. If the forces $\mathbf{S}_i$ approximate the inverted weight distribution of a specimen, the latter can in fact be supported by the load tree, and gravity can be compensated.

In fact, specimen suspension from a load tree naturally guarantees that the force $\mathbf{S}$ at the top of the hierarchy emerge as needed for the suspension to work,

$$\mathbf{S} = \mathbf{W}_s + \Sigma \mathbf{S}_i \tag{1}$$

with $\mathbf{W}_s$ the suspension system weight. Forces $\mathbf{S}_i$ collectively balance specimen weight: each supports one part of the specimen, Fig. 7. Balance about the external support requires vertical alignment between the system centroid and the top fly beam fulcrum location, precisely achievable by adjusting the latter in the actual hardware.

An object so suspended "feels" no gravity to the extent of how fine the $\mathbf{S}_i$ force distribution is. This scenario is similar to a kinetic mobile in the artistic sense of Gabo, Moholy-Nagy, and Calder, Figs. 8 and 9, except the suspended elements are here connected and thus do not float apart, unlike the components in kinetic art. The floating motion in kinetic displays, however, nicely highlights the similarity between the kinematic constraint enforced by a load tree and weightlessness.

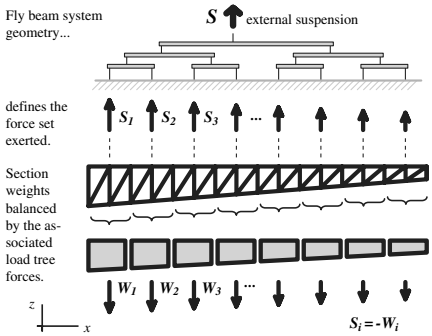

Fig. 7 Weightlessness is simulated if the forces exerted on the specimen balance weights.

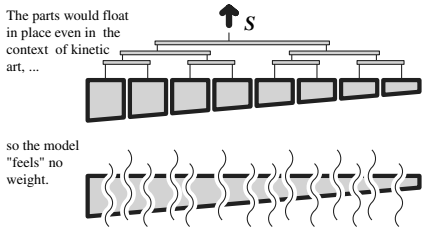

Fig. 8 Each force exerted at the base of the load tree suspends one part of the whole.

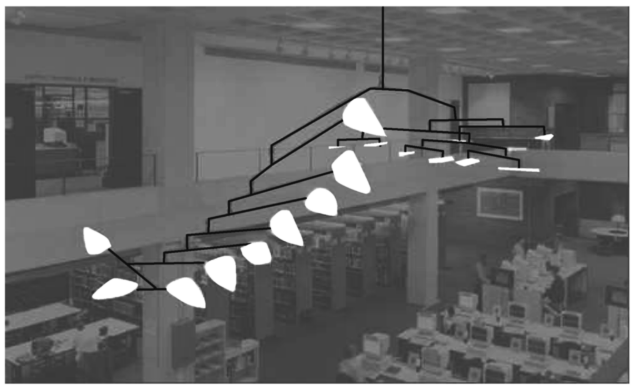

Fig. 9 A. Calder: Mobile, 1963 (Healey Library, University of Massachusetts, Boston).

B. Load Tree as a Constraint Mechanism

To study how a load tree constrains a suspended object, consider kinematics in the gravity direction z and focus on a single fly beam first. As a result of its static determinacy, the attachment of a fly beam, and of subsequent ones, to a mechanical system cannot by itself impose constraints. Thus whatever constraint is exercised by a load tree is ultimately due not to the system of beams but to the hierarchy's external support which suppresses exactly 1 degree of freedom. The fly beams merely transform this singular constraint to the collective context of the anchor points on the specimen.

To study this transformation, consider an ideal fly beam, shown in Fig. 10 with its geometric skeleton subtended by the arm tips $\mathbf{A}_i$ and the fulcrum $\mathbf{F}$. Points $\mathbf{A}_i'$ indicate position with an α tilt, and $\mathbf{S}_i$ denote the suspended weights. Also, for simplicity, ignore the beam mass, a realistic approximation in many practical cases as seen below.

By virtue of the similarity $\mathbf{A}_1'\mathbf{B}_1\mathbf{F}\Delta \sim \mathbf{A}_2'\mathbf{B}_2\mathbf{F}\Delta$, the arm ratio λ

$$\lambda = r_1/r_2 \tag{2}$$

also relates tip vertical displacements h_i and, by moment equilibrium, the loads $\mathbf{S}_i$ and the suspended masses

$$h_1/h_2 = \lambda \tag{3}$$

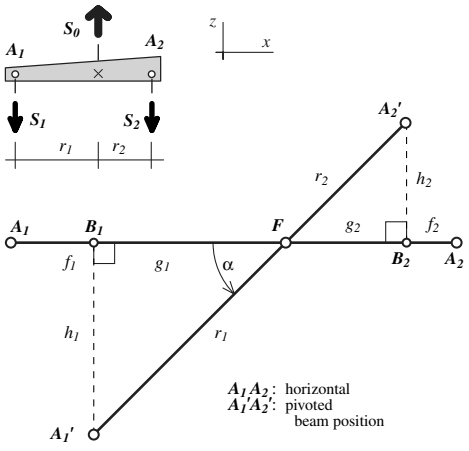

Fig. 10 Fly beam geometric skeleton.

$$\mathbf{S}_2/\mathbf{S}_1 = \lambda \tag{4}$$

$$\mathbf{m}_2/\mathbf{m}_1 = \lambda \tag{5}$$

These relations are independent of the tilt α.

Next observe that, as the tip vertical displacements h_i directly reflect those of masses $\mathbf{m}_i$ $(i = 1, 2)$, the dz_{cg} displacement in the z direction of the *combined* (resultant) center of gravity of *both* suspended systems is

$$dz_{cg} = dz_F + \frac{h_2 m_2 - h_1 m_1}{m_1 + m_2} \tag{6}$$

with dz_F the fulcrum vertical displacement and the signs according to Fig. 10. Finally, combine Eqs. (3) and (5), subsequently rewrite Eq. (6)

$$h_2 m_2 = h_1 m_1 \tag{7}$$

$$dz_{cg} = dz_F \tag{8}$$

and observe that fly beam pivoting does not affect the z height of the center of gravity of the suspended masses. Fulcrum support, $dz_F = 0$, thus constrains the height of the combined center of gravity of the suspended subsystems.

Repetitively applying this principle through the hierarchy, one sees that the load tree simply keeps the specimen center of gravity stationary, a condition equivalent to weightlessness (the principle of the preservation of momentum alone constrains a mechanical system in free flight). Remarkably, this conclusion does not depend on the topology and geometry of the fly beam hierarchy. Specimen response, therefore, should be little affected by the load tree design, as long as a single hierarchy is used with support at the top fulcrum only.

Finally, note that rigorously accounting for fly beam weight would affect the above conclusion in one respect only: by making it apparent that the constraint is applied to the center of gravity of the *combined specimen-suspension system*, not of the specimen alone. The load tree thus effectively frees the specimen from gravitational effects without imposing deleterious kinematic constraints on it. In return, it adds its own mass to the system. This parasitic effect is often negligible and can always be precisely quantified and modeled. (Other parasitic effects would also be added if they were present. However, some of these effects, friction, damping, material stiffness, are virtually nonexistent in a fly beam hierarchy, while the others, second order effects, can be easily eliminated.)

C. Concept Demonstrate: Hardware Model

To demonstration the paradigm's predicted functionality and its independence of load tree design, breadboard hardware models of two different load trees suspending similar beam specimens have been built: one with symmetric, the other with asymmetric topology and geometry, Figs. 11a and 11b. The specimens, 81.3 cm (32 in.) long, 1.5×1.5 mm ($\approx 60 \times 60$ mil) wooden rods, have been made heavier with pairs of steel nuts attached at every inch to increase mass, Fig. 12. The fly beams, connected with lines of sawing thread, have been cut from the same stock except near the top of the hierarchy where the cross sections are larger.

Dominant vibrations, support and specimen imperfection effects, fulcrum offsets, and responses to some external loads have been studied. Theoretical predictions of behavior have been qualitatively verified and practicalities of operation and fabrication have been developed and refined, summarized, in part, in Sec. III.

As foreseen, transient and static responses to like loads differed little between the models, and vibration reflected the features of characteristic free–free beam dynamics. Responses to the same midspan loads are shown in Figs. 11a and 11b.

D. Concept Demonstration: Finite Element (FE) Analysis

For numerical concept verification, a 2 mm thick 2×2 m steel plate ($E = 200$ GPa, $\nu = 0.3$, $\rho = 7800$ kg/m^3, total mass $m_{\text{spec}} = 62.4$ kg) has been modeled with a 20×20 mesh of NASTRAN CQUADR elements. The first three modes of free vibration are shown in Fig. 13.

For the suspension, anchor points at a regular 10×10 grid, each bearing the weight of a 20×20 cm plate area, have been defined. (Note that, while this support pattern is straightforward, it does not rigorously minimize any specimen response—strain, stress, or deflection—to gravity.) Subsequently, a fly beam hierarchy of rank 6 has been designed without any optimization, Fig. 14. Beam box cross sections, all with wall thickness $t = 0.8$ mm, are uniform for each rank, with cross section outer widths $w = 2, 3, 4, 6, 8$, and 10 mm and depths $h = 4$, 5.5, 8. 15, 20, and 25 mm for ranks 1 and up, respectively. High performance graphite composite material has been assumed, $E = 200$ GPa, $\nu = 0.3$, $\rho = 1550$ kg/m^3. Each fulcrum has been placed to balance the suspended weights *combined with* the fly beam weight itself. The total mass of all fly beams is $m_{\text{fb}} = 211$ g. Beams of various ranks have been vertically spaced with $l_c = 20$ cm gaps between ranks, connected with $d = 4$ mil diameter unidirectional graphite fiber cords: $E = 400$ GPa, $\rho = 1650$ kg/m^2. (This small diameter has been used even for the higher ranks to better demonstrate low frequency support compliance vibration.)

As the total mass of all suspending cords turned out to be negligible (≈ 0.1 mg), the mass overhead of the support system, with joints and other details ignored, is

$$m_+ = m_{\text{fb}}/m_{\text{spec}} = 0.211/62.4 \approx 3.4\% \tag{9}$$

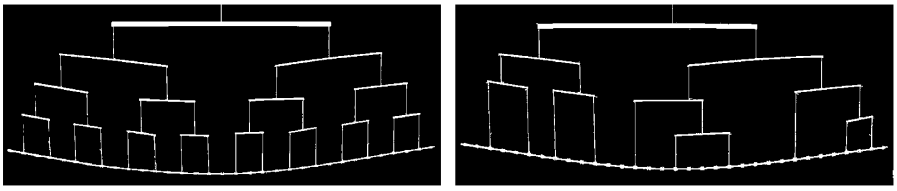

a) Symmetric load tree (whiffle tree) **b) Asymmetric load tree**

Fig. 11 Breadboard demonstration models: silhouettes of deformed shapes (digitally enhanced photos).

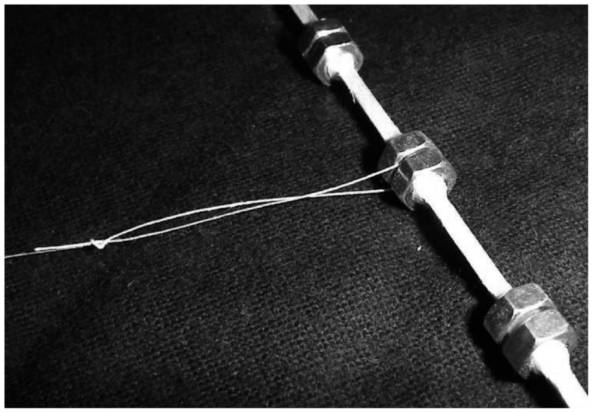

Fig. 12 Model detail: beam anchor point.

Fly beam arms and cord sections between subsequent hierarchy ranks have been meshed with three BAR (uniform beam) elements each. Thus the finite element analysis (FEA) mesh involved 400 plate and 327 bar elements.

As seen from the vibration frequencies in Figs. 13 and 14, the suspension, indeed, well simulates weightlessness: the suspended system frequencies are 1–2% off the free modes. Numerical problems may also have played a role in this discrepancy; the modal analysis of the suspended system has been plagued by iteration errors.

In addition to the faithful simulation of weightlessness, load tree suspension also adds pendulum and internal compliance modes that should not be allowed to interfere with the specimen modes of interest. For the plate model, mode separation has been sufficient for the five pendulum modes, three of which are shown in Fig. 15. [Modes 3 and 5, not shown, are swing and tilt modes like 2 and 4 (Figs. 15b and 15c) in the complementary direction.] However, the dominant support compliance mode, vertical system vibration, Fig. 16a, with $f = 1.441$ Hz, is close to the first free mode, Fig. 14a, $f = 1.655$ Hz. Interference between the two could be avoided by altering suspension system stiffness. Cord stiffness could be increased with negligible penalty; however, fly beam stiffness costs more weight, unless an optimized beam design is used.

Vertical fulcrum offsets are zero for all undeformed beams except the top one, where $e_z = 1$ mm (Fig. 17) for tilt stability. In the context of this offset, the small error in the horizontal fulcrum location $e_x \neq 0$ in the same beam, the result of numerical error in the calculation of fulcrum position, is sufficient to tilt the system in response to gravity alone, shown amplified in Fig. 16b. This effect

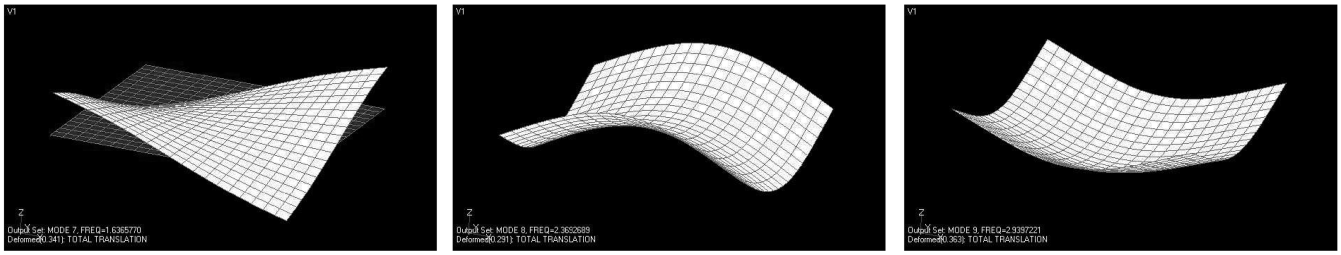

a) Mode 1: *f* = *1.637* Hz **b) Mode 2: *f* = *2.369* Hz** **c) Mode 3: *f* = *2.939* Hz**

Fig. 13 Free-flying 2 mm thick 2 × 2 m steel plate, the first three vibration modes.

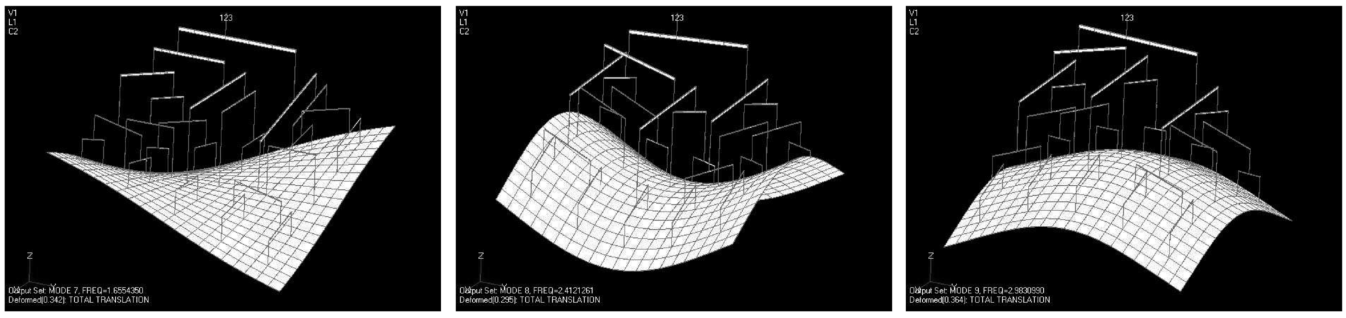

a) Mode 7: *f* = *1.655* Hz **b) Mode 8: *f* = *2.412* Hz** **c) Mode 9: *f* = *2.983* Hz**

Fig. 14 Plate suspended with load tree in gravity field, dominant free vibration modes. (Modes 8 and 9 match Figs. 13b and 13c, displacements negated.)

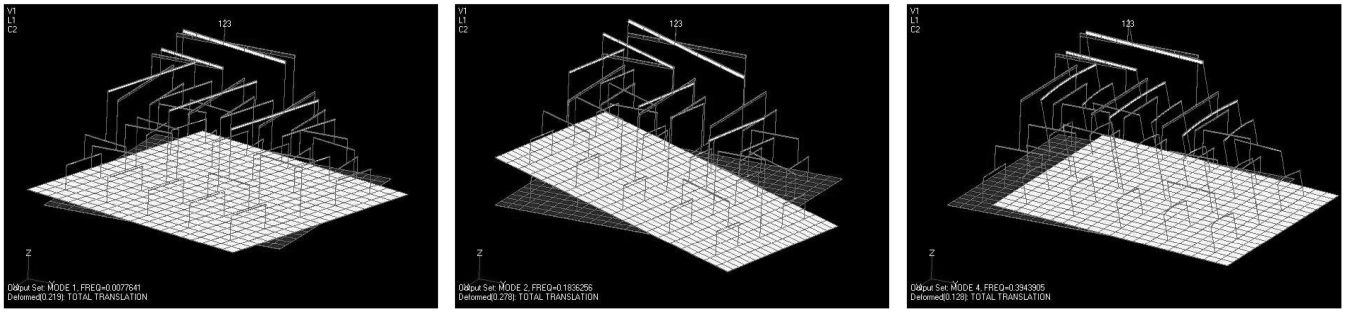

a) Mode 1: yaw, *f* = *0.0078* Hz **b) Mode 2: tilt, *f* = *0.184* Hz** **c) Mode 4: swing, *f* = *0.394* Hz**

Fig. 15 Plate suspended with load tree in gravity field, pendulum modes of vibration.

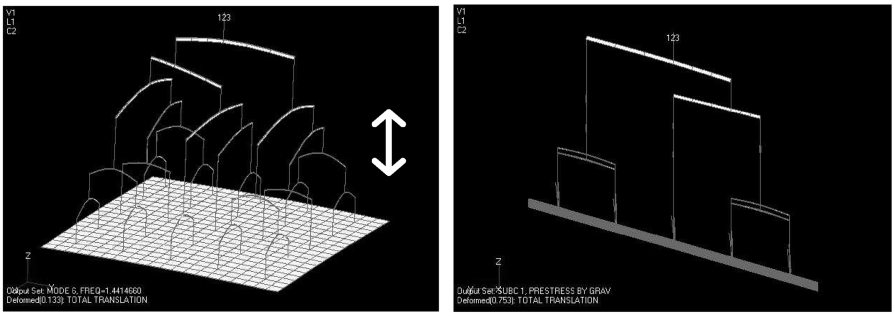

a) Mode 6: $f = 1.441$ Hz b) Response to gravity, side view

Fig. 16 Suspension effects.

highlights system sensitivity to the top beam fulcrum position, discussed in more detail later.

III. Discussion

A. Support Singularity: Single vs Multiple Fly Beam Hierarchies

To physically illuminate the importance of the singularity of external support, consider the opposite: multiple beam hierarchies (suspension from more than one external point). In this case, as seen above, each hierarchy constrains the center of gravity of the parts it suspends, not that of the full system. All motion to involve the displacement of any of these "local" centroids is directly affected, including rigid body rotation (global tilt), most vibration modes, and responses to internal effects, Fig. 18. Weightlessness is no longer simulated.

B. Light Cantilevers, Spacecraft Booms

It is educational to consider the support of a light boom attached to a heavy base (a spacecraft bus). As in other cases, for the suspension to work, the load tree geometry has to simply reflect the specimen mass distribution which is rather nonuniform in this case, Fig. 19a. (To avoid fulcrum offset effects described below, care must be taken to effectively suspend the bus at its centroid, rather than on its exposed upper face.)

If the bus were replaced with a fixed support, then all kinematics involving bus motion would be affected, even if this involvement were small. Support should no longer be exercised with the load tree

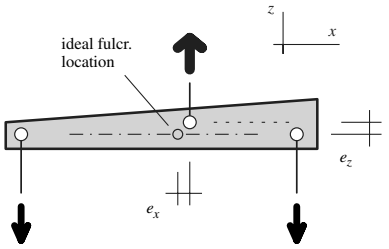

Fig. 17 Fulcrum offsets.

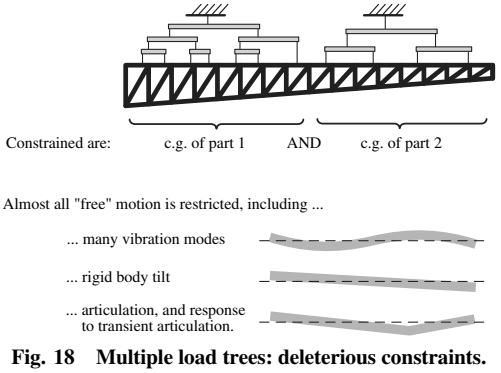

Fig. 18 Multiple load trees: deleterious constraints.

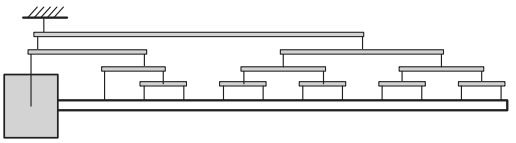

a) Marionette support: support with one load tree

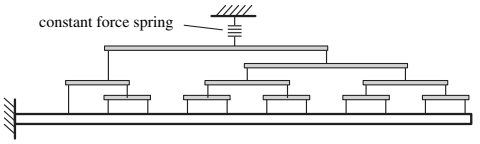

b) Load tree as force distribution device

Fig. 19 Alternative test setups for cantilever system.

but, instead, the latter should be used as a classic load distribution device, Fig. 19b. This test setup is no longer the Marionette paradigm.

C. Horizontal Dynamics

A fly beam cannot only pivot ("pitch"), but also horizontally rotate ("yaw") about its fulcrum virtually unconstrained, if the torsional stiffness of the suspending cord is near zero as one would expect. Consequently, a load tree can also freely accommodate lateral specimen kinematics with local motion perpendicular, rather than parallel, to the fly beams involved, such as the small to moderate horizontal dynamics of a straight beam, Fig. 11. Global pendulum effects do not arise because the system center of gravity remains exactly under the top support, lest horizontal momentum would not be preserved. Local pendulum effects within the hierarchy do not occur either because all cords remain vertical (for small to moderate motion): the fly beam horizontal rotations accommodate beam deformations.

Lateral specimen motion, however, can excite fly beam horizontal swinging or may be too fast for the beams to adjust to in a timely manner. The first scenario involves beam transient, the latter pendulum, effects: either may seriously compromise test results. Horizontal dynamics, therefore, have to be carefully considered. Global suspension design (topology and geometry), fly beam masses, as well as cord tension (specimen weight associated with each anchor point) all influence the described effects and are, therefore, all available to either mitigate or eliminate their deleterious impact. Of course, if specimen dynamics are limited to the vertical (suspension) direction (e.g., the steel plate modeled above, Fig. 14) then horizontal dynamics is not an issue.

D. Material Interference With Specimen Response

Apart from precisely quantifiable inertial effects, the Marionette suspension little interferes with specimen response. Having no deforming components, the hierarchy does not contribute to damping or materially affect stiffness. There is no free play (slack), a

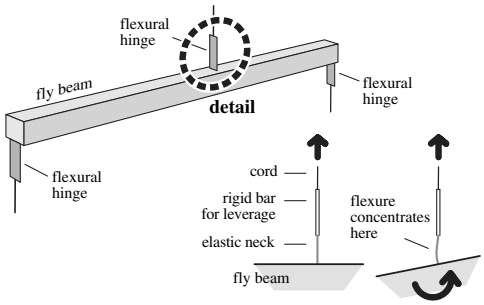

Fig. 20 Frictionless hinge (thin elastic flexure).

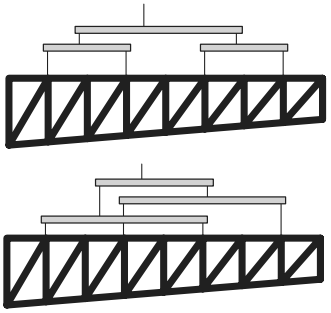

Fig. 21 Kinematically equivalent alternatives.

problem in many precision systems. Friction at the cord anchor points, the only material effect to possibly pollute system response with uncertainty, is benign by nature. Besides, even this friction can be virtually eliminated with flexure joints, compliant elastic tongues, Fig. 20, that avoid even the minor energy dissipation associated with cord bending.

E. Robustly Flexible Design

The one qualifying feature of the Marionette paradigm is singular support: one suspending load tree. The architecture is limited by no other rule or principle, except for generic design considerations. Support design is, therefore, robustly flexible. For example, either option in Fig. 21, even the one with overlapping subhierarchies, is kinematically acceptable.

F. Geometric Nonlinear Stiffness: Fulcrum Offsets

With its negligible length error ignored, a fly beam's geometric imperfections reduce to the fulcrum offset e from its ideal location, Fig. 17. The horizontal component of this offset, e_x, alters the ratio of beam tip forces $\mathbf{S}_1$ and $\mathbf{S}_2$, Fig. 10, a perturbation to ultimately affect specimen support force distribution. As a result, the specimen's internal loads (bending, shear, etc.) as well as its static deformations become somewhat different from those planned. (The deformation difference may even be perceivable for an extremely compliant structure.) Dynamic performance of specimen and support, however, remain unaffected.

The top fly beam, however, may tilt (with the entire system) as a result of a nonzero e_x, compare to Fig. 16b. This effect can be naturally controlled with precise fulcrum adjustment, a correction necessitated by the imperfections not only of fly beam geometries but also of specimen and fly beam mass distributions.

A vertical fulcrum offset e_z, however, introduces a rotational stiffness K_α by effecting an M torque proportional to the tilt α and the fulcrum load $\mathbf{S}$

$$M = K_\alpha \alpha \tag{10}$$

$$K_\alpha = e_z \mathbf{S} \tag{11}$$

Moment M is a restoring torque ($K_\alpha > 0$) if $e_z > 0$ (the fulcrum is above its ideal location) whereas it is a destabilizing one ($K_\alpha < 0$) otherwise. A stiffness K_α is introduced to each fly beam with a vertically offset fulcrum location. The cumulative effect of all these stiffnesses over the entire hierarchy may be a concern, especially if the offset errors are systematic. This results if, for example, fly beam design does not account for deformations under load (linear theory). In this case the fulcra, with no vertical offsets beyond fabrication errors in the unloaded state, develop uniformly positive offsets under load. Nonlinear design, however, is not the only means to control this geometric stiffness effect. An additional, and perhaps more effective, means of control is precision vertical fulcrum adjustment in all fly beams.

A positive vertical fulcrum offset $e_z > 0$ in the top beam, however, should be maintained for system robustness to softly support with a restoring torque the top beam against tilt. (A negative offset, no matter how small, would destabilize the system by increasing global tilt until system integrity is lost.) However, the offset's net effect on the specimen is not necessarily a support against pitch rigid body rotation since the latter is equivalent with top fly beam tilt only in certain symmetric configurations. (For instance, the first, symmetric, vibration mode of the specimen in Fig. 11b still involves some, albeit minor, top fly beam tilt due to the asymmetry of support.)

Insensitivity to general horizontal fulcrum offsets and the ease of control of both vertical and horizontal ones via fulcrum adjustment renders the support system fault tolerant. As control can be exercised in the operational state with simple mechanical means and to geometric precision, this fault tolerance is robust.

G. Force Fields Other than "Pure" Weightlessness

Marionette support does not prohibit the use of load trees in addition to the suspending one if the former work strictly as load distribution devices, not as supports. Such a scenario is shown in Fig. 22, where the suspending hierarchy supports system weight and an extra force field combined. (To avoid proportionally increasing system mass when applying this field, one may use constant force devices, rather than a weight hung on the loading hierarchies.) The extra forces can be designed to make the setup simulate steady state acceleration or other load bearing conditions such as the state during certain slew maneuvers.

H. Moderate to Large Deformations

For an articulated specimen such as a robotic system, the topology of the beam hierarchy may reflect specimen articulation to accommodate moderate to large kinematics. For example, a person suspended with a hierarchy interlinked akin to the human skeleton, Fig. 23, would experience the same global response as in space even to large limb motion.

I. Hardware Safety: Support Redundancy

Lack of support redundancy in the Marionette system may raise risk concerns when expensive hardware is tested. Should, for a test, safety be more acute a concern than for similarly nonredundant suspension devices for sensitive high-tech hardware (cf. Fig. 6) or in high risk environments with little control over the operation (construction cranes), hardware safety can be enhanced via a number of simple means. For example, the top fly beam could be supported not from above with a tether but with a robust beam from underneath; it could "rest" on this cross beam with a precision rolling interface or a pin to permit free tilt and rotation. Also, "seat belts" of elastic-

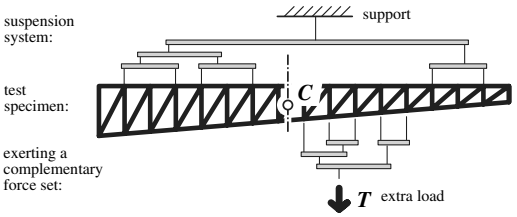

Fig. 22 Loads applied with secondary load tree.

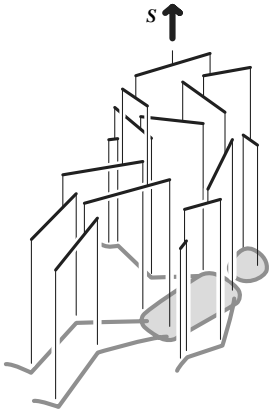

Fig. 23 Space experience.

ductile cables or other elements could be arranged (e.g., hung from above) under critical fly beams without contact but ready to softly catch the component if needed. Also, the specimen could rest on a stand (perhaps where it had been assembled) at all times except for the brief periods of fly beam fulcrum adjustment and the testing itself, when it would be temporarily lifted as if by a crane.

J. Adaptive and Expanding Geometries

The replacement of (some) fly beams with mechanisms of adaptive length may enable the Marionette paradigm to follow without pendulum effects certain types of evolution of specimen geometries. A straightforward option is the use of the pantograph mechanism, Fig. 24, because its internal kinematics maintains fly beam arm proportions and, therefore, does not interfere with the overall load tree design. If dynamics not only at various stages of specimen reconfiguration but also during the process (e.g., deployment) are to be tested, then friction in mechanisms as in Fig. 24 must be controlled, perhaps with active deployment control for each scissor element.

IV. Performance, Optimization

Because of its simplicity and robust fault tolerance, apparatus design and fabrication for Marionette suspension can often be carried out by simple and approximate means. However, system optimization for best performance, for minimal inertial interference with specimen response, is difficult.

To minimize support-specimen inertial interference, this effect should first be quantified with a rigorously defined merit function. Preferably, this function should be rapidly assessable to easily compare the performances of preliminary alternatives (e.g., different load tree topologies and specimen anchor point distributions). Finally, once the best topology and an approximate geometry have been identified, detailed optimization should pin down the final design. These steps and the merit function itself should recognize that the inertial interference is influenced *collectively* by 1) the distributions of specimen mass and of the anchor points, 2) the specimen kinematics (e.g., vibration modes) of interest, 3) the topology and geometry of the beam hierarchy, and 4) the fly beam designs. These effects are complex by themselves; a formal and general treatment of their mutual interaction would be difficult.

To qualitatively illuminate this complexity, consider how fly beams and specimen kinematics couple during the vibration of the model in Fig. 11. Clearly, beams at the base of the hierarchy move with the specimen, they directly participate in its kinematics, for all major modes. (The participation of a rank 1 beam diminishes only if its specimen anchor points are near the vibration shape nodal locations, a scenario likely associated with high frequencies.) Although beam mass generally increases with rank number, participation in specimen kinematics gets increasingly attenuated and dependent on the kinematics itself. For example, the heaviest, top, beam in Fig. 11a does not move at all during specimen vibration with the first, symmetric mode while it participates in the second, antisymmetric mode. In contrast, the top beam in the alternative design, Fig. 11b, is involved in both the first and the second modes. Of the two designs, however, the second is lighter due to its fewer anchor points and beams.

Clearly, suspension system mass is not a rigorous measure of inertial pollution: the latter also depends on specimen kinematics, anchor point distribution, load tree topology, etc. Nevertheless, support mass can still be used as a conservative indirect indicator of parasitic inertia. Conservative because, of the total mass included in this blank measure, only a portion really matters, and in this portion it is the lightest, lowest rank, beams that are most fully represented. This measure is also indirect, because it ignores the interaction between the various aspects of support design and specimen response.

Despite these flaws, however, mass is an attractively simple metric. In fact, its simplicity is why it is used as a first approximation of support performance in the study discussed below. However, besides using this metric, this study is also limited (rendered even more conservative) by not considering the variations of anchor point distribution and load tree topology. As a result, system optimization is reduced to that of the individual fly beams: the general study of a single fly beam (repetitively applicable through the hierarchy) illuminates the problem at large. This approach is justified by the purpose of the study: a simple indication of the practicability of the Marionette concept is sought, not the assessment of ultimate performance.

A. Fly Beam Engineering: General Considerations

Fly beam design, whether embedded in rigorous global optimization or an independent module as in the study below, attempts to minimize inertia and to eliminate second order effects. The former objective, inertia minimization, may distinguish (in the beam context) between mass and mass moment of inertia. As the latter quantity penalizes mass with the square of the distance from the axis of rotation, its minimization results in beams more slender than designs for lowest mass. The relative importance of the two

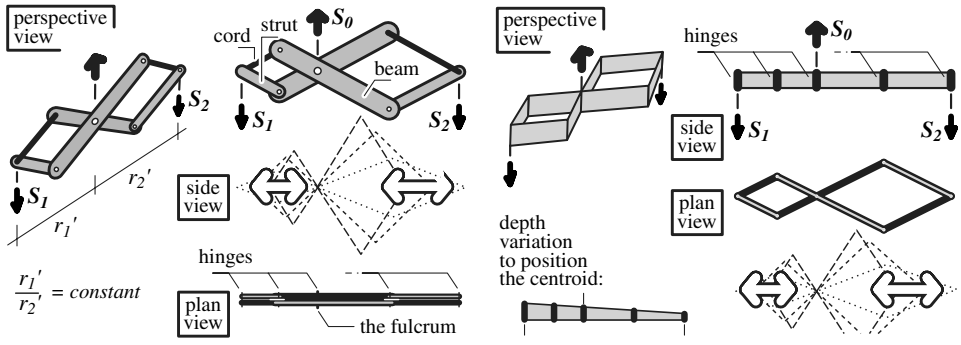

a) Vertically scissoring mechanism **b) Horizontally scissoring mechanism**

Fig. 24 Variable-length pantographic fly beam.

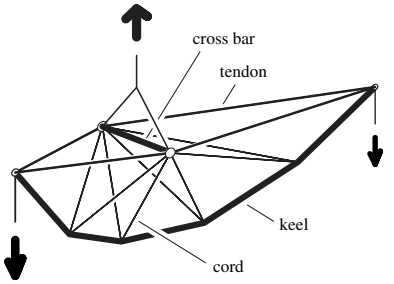

a) Architecture for least mass.

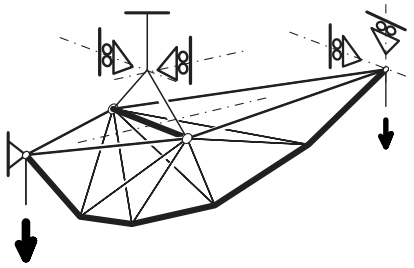

b) Support for linear FEA.

Fig. 25 Single keel beam with bipod suspension.

quantities depends on how the beam translates and pivots (or, whether it translates or pivots) as the load tree moves; this motion, in turn, depends on the specimen kinematics itself. In the study below, only beam mass is considered without rotational inertia.

The other design objective, the elimination of second order effects, can generally be achieved simply with fulcrum adjustment after fabrication. Success depends on the precisions of design, fabrication, and postfabrication calibration. In terms of the design, the nonlinear nature of the problem needs to be kept in mind. The ideal fulcrum location (the center of gravity of beam and beam tip masses combined) depends both on the beam design itself and also on the loads applied because the latter can considerably deform a fly beam mass optimized without stiffness constraints. The fulcrum should move to its appropriate location with the beam deforming when loaded.

B. Fly Beam Architecture for Minimum Mass

In a concept development study, trusslike fly beam architectures have been developed for minimum mass, minimum mass moment of inertia, as well as for the precisely linear arrangement of center of gravity (fulcrum) and beam tips. The most promising designs have also been modeled as breadboard demonstration hardware to study fabrication techniques, performance, and overall robustness. Of these, the mass-optimized architecture of Fig. 25 has been chosen for detailed study.

The backbone of this structure, in its plane of symmetry, is a keel of straight segments to connect the fly beam tips as a compressed arc. The number of segments is herein referred to as the *keel number*. The joints between the segments are hinges in the plane of symmetry but are flexurally stiff laterally to resist keel buckling. Further lateral support is provided by the cords that symmetrically anchor the keel to the *cross bar* endpoints which, in turn, define the fulcrum, suspended with a pair of cords. The cords that connect the cross bar to the beam tips bear more tension than the rest and are referred to as *tendons*.

C. Design Specifications

For the parametric study, beam design specifications to reflect material and technological qualities likely achievable with fabrication and operation in a well-controlled environment have been used. Imperfections, not quantified, have been indirectly accounted for via factors of safety of at least two, $FS \geq 2$, in all failure criteria.

1. *Material and Technological Properties*

Keel segments and cross bar: Tubular construction from generic composite material is assumed; $E = 10$ Msi, $\nu = 0.3$, and $\rho = 1600$ kg/m^3. Wall thickness and tube diameter are continuously variable from minima $t_{\min} = 2$ mil and $d_{\min} = 8$ mil up, respectively. Member slenderness ratios are at most $l/d \leq 120$.

Cords and tendons: Unidirectional fibers with little resin are used: $E = 15$ Msi, $\rho = 1500$ kg/m^3, with strength $R_u = 350$ ksi. Cord and tendon diameters are continuously variable from minima $d_{\min,\text{cord}} = 0.5$ mil and $d_{\min,\text{tendon}} = 2$ mil up, respectively.

Keel joints: Each joint between two keel segments has zero and infinite flexural stiffnesses in the keel plane and laterally, respectively, and its mass is a function of the fly beam span $m_{\text{keel}} = L \times 0.5$ g/m. The other joints (at the keel and crossbar ends) are 3 times heavier.

2. *Failure Criteria*

Keel segments and cross bar: The standard strut failure modes of local (tube wall) and global (Euler) stability are considered [12]. Cross bar length cannot be less than 5% of fly beam span.

The entire keel: Lateral loss of global stability is modeled with an equivalent beam on an elastic foundation. Foundation stiffness is the average lateral stiffness provided by the cords, and pin support at the beam ends is assumed to reflect high tendon stiffness. Compression is the average segment load and the beam length is the sum of all segment lengths.

Cords and tendons: Cord and tendon snap are considered. For keel tip lateral support, tendon diameters at least 8 times that of the cords are used. (As tensile failure generally turns out to not be critical, tendon and cord diameters are $d_{\text{tendon}} = 4$ mil and $d_{\text{cord}} = 0.5$ mil, respectively, in most designs.)

D. Design Study

1. *Design Procedure*

In the parametric study performed, design has been carried out with dedicated software featuring nested optimization and embedded FEA. The solution algorithm, on the top level, begins with incrementing the keel number and generating for each a feasible fly beam truss topology. The best geometry for each topology is pinned down next with optimization, performed with the free COBYLA software package, using total mass as the objective function. The search is constrained by the keel global stability criterion and by requiring zero reaction forces at supports that are artificially introduced, Fig. 25b, to render the mechanical model statically determinate and thus solvable with cheap linear FEA. Truss member (strut and cord) failure criteria are addressed with an embedded optimized design carried out for the FEA-based member loads. Once the best geometries for all reasonable keel numbers are selected, the most weight-efficient design of these is selected.

2. *Parametric Study*

Besides the general specifications spelled out above, the design problem for each fly beam has been defined with the beam span L as well as the sum $\mathbf{S} = (\mathbf{S}_1 + \mathbf{S}_2)$ and the ratio of the arm loads $\phi = S_1/S_2$. (Total load $\mathbf{S} = 5$ N and force ratio $\phi = 4$, for instance, define arm loads $\mathbf{S}_1 = 4$ N and $\mathbf{S}_2 = 1$ N.) The parametric space to

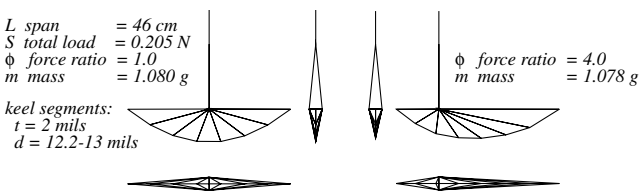

Fig. 26 Optimal design examples for a light beam.

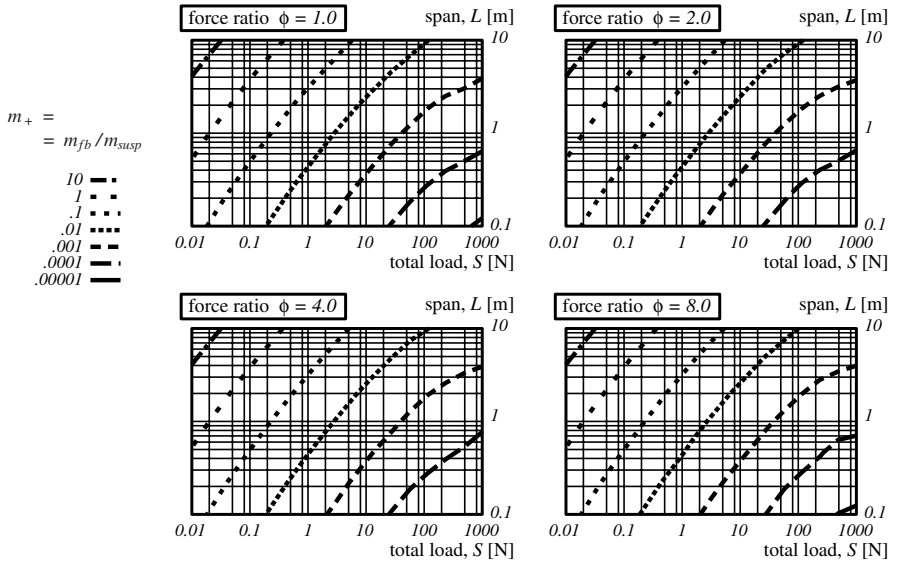

Fig. 27 Direct mass overhead $m_+ = m_{\rm fb}/m_{\rm susp}$ of optimized fly beams.

be mapped has been chosen with a wide range of practical needs in mind. Namely, spans $L = 10$ cm $\cdots$ 10 m, total supported loads $S = 0.001 \cdots 1000$ N, and force ratios $\phi = 1 \cdots 8$, with six, sixteen, and four logarithmic steps each, have been used. Consequently, optimized fly beam design has been carried out for 364 combinations of L, S, and ϕ. Repeated optimization has been necessary for a number of designs to finally succeed, and there have even been times where the effort was ultimately abandoned.

Two characteristic examples of successful design, lightly loaded short beams with identical span $L = 46$ cm and total load $\mathbf{S} = 0.205$ N but different force ratios $\phi = 1$ and 4 are shown with key parameters in Fig. 26. The masses ($\approx$1.08 g) and keel shapes are nearly identical, little affected by the force ratio.

The results of the parametric study are shown in Fig. 27 via the ratio of the beam mass to that suspended, the *direct mass overhead* $m_+ = m_{\rm fb}/m_{\rm susp}$ evaluated on Earth (in a 1-g environment).

The lower this overhead, the more efficient the design. On all four plots (one for each force ratio considered), the direct mass overhead is plotted against the supported load $\mathbf{S}$ and the beam span.

A striking feature of the plots is their similarity: the results little depend on the force ratio λ. Apparently, besides span, it is the total load only, not the manner in which it is divided between the beam tips, that matters. The reason for this phenomenon, also apparent in the example of Fig. 26, has not been identified.

It is also apparent that the mass overhead increases for large spans and light loads, with the best performance (the lowest overhead) achieved in the opposite scenario: short, heavily loaded beams. Although the actual values plotted are specific to the beam architecture, technological assumptions, and acceleration of gravity, this trend is general.

Most importantly, however, the results reveal that the fly beam mass overhead is minor in many practical cases. For example, the suspension over a 4 m span of 20 N weight ($\approx$2.0 kg suspended mass) only involves about 1% fly beam mass overhead, an example of midrange performance well between the extremes plotted. A more efficient example is 1 m span, 100 N suspended weight ($\approx$10.2 kg mass) and roughly 6×10^{-4} overhead. Such overheads, even when repetitively combined through the load tree ranks (e.g., six repetitions for the specimen in Fig. 13), have minor inertial impact. The overhead is seen even less deleterious recalling that participation in specimen kinematics diminishes with beam rank and, for tests conducted to validate FEA, it is the precise quantification, not the magnitude, of inertial pollution that matters most.

As also seen from the plots, very lightly loaded beams, especially with large spans, can even weigh more than the loads carried. For example, 5 m span and 0.05 N suspended weight ($\approx$5.1 g mass) implies a beam about 2.5 times heavier. The engineering of such a fly beam, in fact, is driven not by the loads but by technological limits, taken to reflect common laboratory techniques in the present study. Consequently, there is room, perhaps much room, to improve this performance if necessary.

V. Summary

The Marionette paradigm, a gravity offloading scheme for the vibration testing of free-flying systems such as spacecraft, has been proposed. The new concept combines mechanical simplicity, high performance, and versatility in testing and test apparatus design. Among its critical features are the lack of frictional and material stiffness interference with specimen response, the easy control of second order effects, robust fault tolerance and design flexibility, the accommodation of moderate to large specimen kinematics in some cases, and the possibility of generalization to horizontally expanding specimen geometries (e.g., for the vibration testing of a specimen at several phases of deployment).

Functionality has been verified with hardware demonstration models and numerical analysis. The fly beam design problem has also been explored in detail, and a parametric design optimization study has been performed to assess the mass overhead associated with fly beam suspension, a conservative estimate of inertial pollution by the Marionette support. This study has shown that the mass overhead is minor for many practical applications and can even be negligible for short, heavily loaded beams. Significant overheads are associated only with very lightly loaded beams, especially those of long span.

The study also revealed that, for the given fly beam architecture considered, beam optimal mass does not depend on how a given total suspended mass is divided between the beam ends.

Acknowledgments

This work has been supported by NASA Langley Research Center, award number NAG-1-03003. The analysis of the plate model for numerical concept verification has been performed with NE/NASTRAN, with a license made available for this effort by L'Garde, Inc. The design study relied on the freely available general optimization package COBYLA. All other software used, including the embedded FE package and the software for nonlinear strut design, was developed by the first author.

References

[1] Fischer, A., and Pellegrino, S., "Interaction Between Gravity Compensation Suspension System and Deployable Structure," *Journal of Spacecraft and Rockets*, Vol. 37, No. 1, Jan.–Feb. 2000, pp. 93–99.

[2] Fischer, A., "Gravity Compensation of Deployable Space Structures," Ph.D. Thesis, Pembroke College, The University of Cambridge, Cambridge, U.K., Nov. 2000.

[3] Menon, C., Busolo, S., Cocuzza, S., Aboudan, A., Bulgarelli, A., Bettanini, C., and Angrilli, F., "Issues and New Solutions for Testing Free-Flying Robots," *55th International Astronautical Congress of the International Astronautical Federation, the International Academy of Astronautics, and the International Institute of Space Law*, IAF, Vancouver, Canada, 2004, IAC-04-J.5.08.

[4] Salama, M., White, C., and Leland, R., "Ground Demonstration Of A Spinning Solar Sail Deployment Concept," *The 42nd AIAA/ASME/ASCE/AHS/ASC Structures, Structural Dynamics, and Materials Conference and AIAA/ASME Adaptive Structures Forum*, AIAA, Reston, VA, 2001; also AIAA Paper 01-1266.

[5] Greschik, G., Mikulas, M. M., and Freeland, R. E., "The Nodal Concept of Deployment and the Scale Model Testing of its Application to a Membrane Antenna," *The 40th AIAA/ASME/ASCE/AHS/ASC Structures, Structural Dynamics, and Materials Conference and AIAA/ASME Adaptive Structures Forum*, AIAA, Reston, VA, 1999; also AIAA Paper 1999-1523.

[6] Barenblatt, G. I., *Scaling, Self-similarity, and Intermediate Asymptotics*, edited by D. G. Crighton, Cambridge Texts in Applied Mathematics No. 14, Cambridge Univ. Press, New York, Dec. 1996.

[7] Straube, T., and Peterson, L. D., "A Large Motion Suspension System for Simulation of Orbital Deployment," *The 35th AIAA/ASME/ASCE/AHS/ASC Structures, Structural Dynamics, and Materials Conference and AIAA/ASME Adaptive Structures Forum*, Vol. 4, AIAA, Washington, D.C., 1994, pp. 1959–1969; also AIAA Paper 94-1568-CP.

[8] Kienholz, D. A., "Simulation of the Zero-Gravity Environment for Dynamic Testing of Structures," *The 19th Space Simulation Conference Cost Effective Testing for the 21st Century*, IES/AIAA/ASTM/NASA/CSA, NASA Goddard Space Flight Center, SuDoc NAS 1.55:3341, NASA-CP-3341, Report 97A00653, 1997, pp. 219–230.

[9] Murphey, T. W., and Mikulas, M. M., "Nonlinear Effects of Material Wrinkles on the Stiffness of Thin Polymer Films," AIAA Paper 1999-1341, 1999.

[10] Adler, A., Hague, N., Spanjers, G., Engberg, B., Goodding, J., David, D. M., and Mikulas, M. M., "PowerSail: The Challenges of Large, Planar, Surface Structures For Space Applications," AIAA Paper 2003-1828, 2003.

[11] Lichodziejewski, D., Derbes, W., Reinert, R., Belvin, K., Slade, K., and Mann, T., "Development and Ground Testing of a Compactly Stowed Scalable Inflatably Deployed Solar Sail," AIAA Paper 2004-1507, 2004.

[12] Anon., "Buckling of Thin-Walled Circular Cylinders," NASA Space Vehicle Design Criteria (Structures) NASA SP-8007, Aug. 1968, revision of September 1965 version.

G. Agnes
Associate Editor